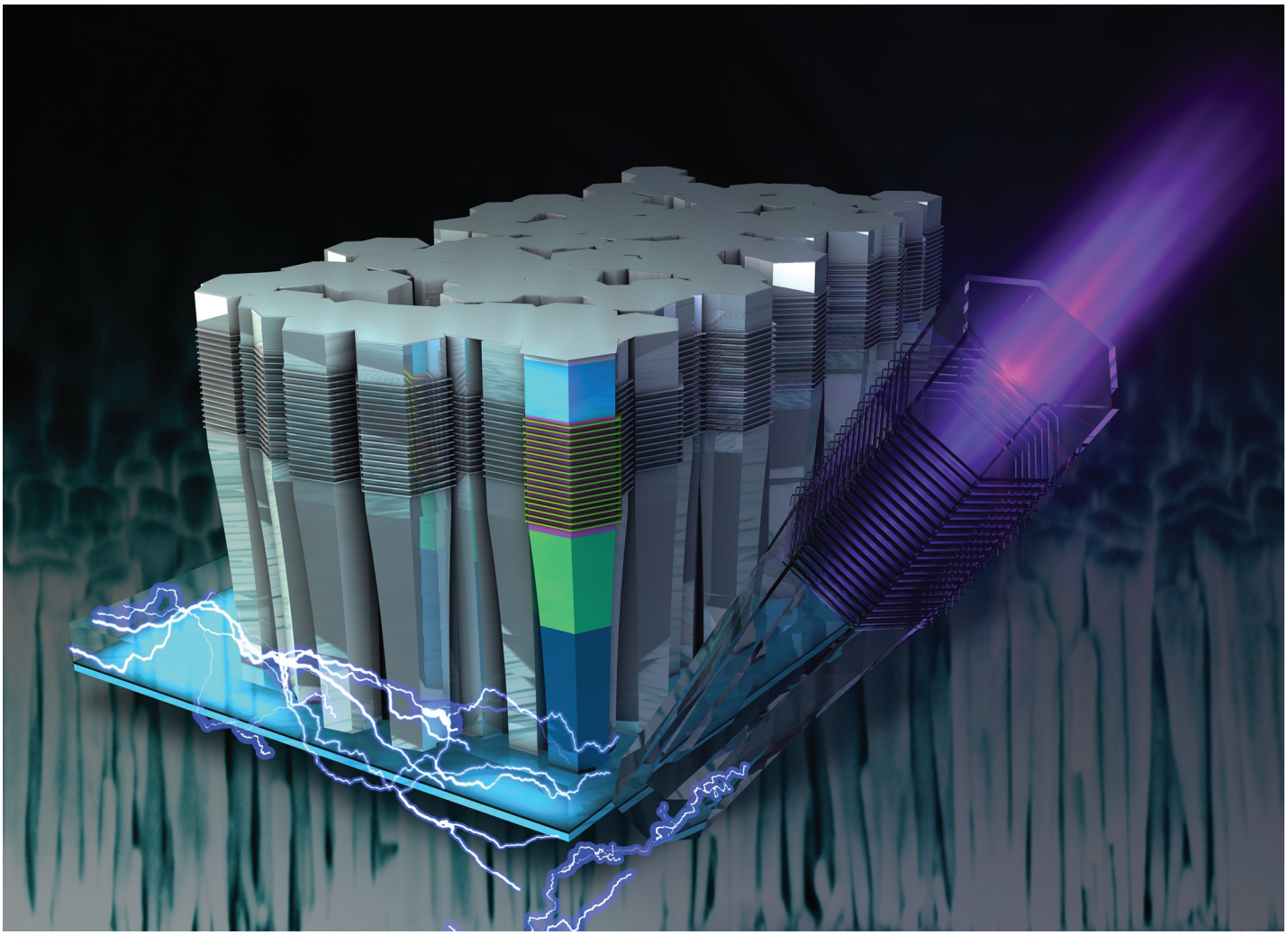

Showcasing research from the Photonics Laboratory, King Abdullah University of Science and Technology (KAUST), Thuwal, Saudi Arabia.

Self-planarized quantum-disks-in-nanowires ultraviolet-B emitters utilizing pendeo-epitaxy

The growth of self-assembled, vertically oriented and uniform nanowires has remained a challenge for efficient light-emitting devices (LED). In this investigation, we utilize a pendeo-epitaxy technique for the top p-GaN layer to achieve a self-planarized quantum disk UV-B LED grown on silicon. In addition, an active region based on quantum-confined nanostructures, called the quantum-disks (Qdisks), was also utilized to increase the radiative recombination rate of the injected carriers. This work demonstrates a viable approach to easily fabricate ultra-thin, efficient UV optoelectronic devices on low-cost and scalable silicon substrates.

As featured in:

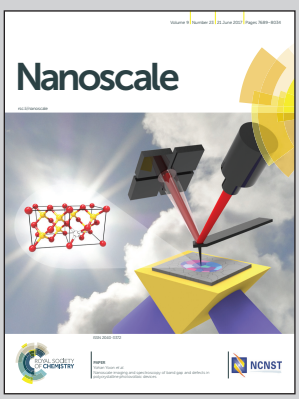

See B. S. Ooi *et al.*, *Nanoscale*, 2017, **9**, 7805.

ROYAL SOCIETY OF CHEMISTRY

rsc.li/nanoscale

Registered charity number: 207890

Nanoscale

PAPER

View Article Online
View Journal | View Issue

Published on 03 March 2017. Downloaded by King Abdullah Univ of Science and Technology on 31/08/2017 13:28:42.

Check for updates

Cite this: *Nanoscale*, 2017, **9**, 7805

Self-planarized quantum-disks-in-nanowires ultraviolet-B emitters utilizing pendeo-epitaxy

B. Janjua,†[a] H. Sun,†[b] C. Zhao,[a] D. H. Anjum,[c] F. Wu,[b] A. A. Alhamoud,[a,d] X. Li,[b] A. M. Albadri,[d] A. Y. Alyamani,[d] M. M. El-Desouki,[d] T. K. Ng[a] and B. S. Ooi*[a]

Received 1st January 2017,
Accepted 24th February 2017

DOI: 10.1039/c7nr00006e

rsc.li/nanoscale

The growth of self-assembled, vertically oriented and uniform nanowires (NWs) has remained a challenge for efficient light-emitting devices. Here, we demonstrate dislocation-free AlGaN NWs with spontaneous coalescence, which are grown by plasma-assisted molecular beam epitaxy on an n-type doped silicon (100) substrate. A high density of NWs (filling factor >95%) was achieved under optimized growth conditions, enabling device fabrication without planarization using ultraviolet (UV)-absorbing polymer materials. UV-B (280–320 nm) light-emitting diodes (LEDs), which emit at ~303 nm with a narrow full width at half maximum (FWHM) (~20 nm) of the emission spectrum, are demonstrated using a large active region ("active region/NW length-ratio" ~50%) embedded with 15 stacks of $Al_xGa_{1-x}N/Al_yGa_{1-y}N$ quantum-disks (Qdisks). To improve the carrier injection, a graded layer is introduced at the AlGaN/GaN interfaces on both p- and n-type regions. This work demonstrates a viable approach to easily fabricate ultra-thin, efficient UV optoelectronic devices on low-cost and scalable silicon substrates.

Introduction

Ultraviolet (UV) light emitting diodes (LEDs) and lasers have attracted considerable attention for applications in sterilization, environmental cleaning, medicine, and lighting, among other fields.[1] AlGaN-based UV LEDs, which cover the spectrum of 210–360 nm, can be used to replace the mercury lamp, which contains environmentally hazardous materials. Although tremendous progress has been made on AlGaN-based light-emitting devices, such as LEDs and lasers, UV emitters still have low illumination power and low efficiency.[2] The unresolved material-related challenges and problems are a lack of efficient p-type doping in high-Al-content AlGaN, high threading dislocations and defect densities in planar UV LEDs grown on foreign substrates, and low light extraction efficiency (less than 10%).[3,4]

Recently, researchers have proposed an alternative pathway to achieve high-efficiency UV LEDs[5] and lasers[6–8] using AlGaN nanowire (NW) structures. Considerable progress has been made in NW-based UV LEDs and lasers because of the superior crystalline quality (dislocation free) of the AlGaN NW and the surface-enhanced p-type dopant (Mg) incorporation.[9] In their simulation, Mehrdad *et al.* recently reported that a light extraction efficiency of up to 70% could be achieved using the NW-based platform due to the light scattering and reduced absorption.[10] However, non-radiative recombination at the surface of the NW structures can be a primary cause of the low internal quantum efficiency (IQE) of InGaN-based NW LEDs due to the high surface-to-volume ratio. The AlGaN core–shell structure, which acts as a self-passivation AlGaN layer, has been reported to provide superior carrier confinement and motivation for realizing high-efficiency UV LEDs.[11,12]

Nevertheless, most AlGaN or InGaN NWs have been grown on foreign substrates.[5,6,13–15] The challenge of their implementation in practical devices is directly related to the fabrication of such NW-based optical devices using a low-cost, scalable and controllable process. Because of the difficulty in controlling the height uniformity, surface morphology of NWs, twist/tilt in crystal orientation and the filling factor of nanostructures, researchers must use polymers for surface planarization to make ohmic contacts. Making good ohmic contacts is even more challenging for UV and deep UV LEDs because of the limited availability of UV-transparent polymers. Recently, Le *et al.* demonstrated the controlled coalescence of an AlGaN NW array on GaN-on-sapphire substrates; however, the process required a substrate-patterning process using a Ti mask to

[a]*King Abdullah University of Science and Technology (KAUST), Photonics Laboratory, Thuwal 23955-6900, Saudi Arabia. E-mail: Boon.ooi@kaust.edu.sa*
[b]*King Abdullah University of Science and Technology (KAUST), Advanced Semiconductor Laboratory, Thuwal 23955-6900, Saudi Arabia*
[c]*King Abdullah University of Science and Technology (KAUST), Imaging and Characterization Core Lab, Thuwal 23955-6900, Saudi Arabia*
[d]*National Center for Nanotechnology, King Abdulaziz City for Science and Technology (KACST), Riyadh, 11442-6086, Kingdom of Saudi Arabia*
† These authors contributed equally to this work.

Published on 03 March 2017. Downloaded by King Abdullah Univ of Science and Technology on 31/08/2017 13:28:42.

achieve high coalescence of AlGaN NWs for the p-type metal deposition.[16] A similar coalescence technique has been adopted for GaN-based nanocolumn UV devices to reduce the fabrication complexity.[17] In addition, the majority of previous AlGaN-based NW devices have focused more on spontaneously formed AlGaN NW heterostructures in the form of either double heterostructures (DHS) using the polarization induced doping configuration[18,19] or the conventional PIN DH structure.[5,6] Few studies have discussed $Al_xGa_{1-x}N/Al_yGa_{1-y}N$ multiple quantum-disks (Qdisks), which should have superior carrier confinement and thus improve the optical performance of the device.[17,20,21]

In this work, we demonstrate high-density, spontaneously coalesced, dislocation-free AlGaN NWs that were grown on a silicon (100) substrate using MBE. The optimized growth conditions enabled us to realize self-planarized NWs with a (0001) orientation and a filling factor greater than 95%. As a result, the p-metal contacts can be formed without the planarization step. Furthermore, we grew 15 pairs of $Al_xGa_{1-x}N/Al_yGa_{1-y}N$ Qdisks, which occupy nearly half the volume of the entire NW, and a notably thin p-type AlGaN electron-blocking layer. Finally, a p-type graded AlGaN layer (~25 nm) and a p-GaN layer (~20 nm) were grown as a top contacting layer. This large ratio of the active region to the entire NW creates more opportunities for the injected electrons and holes to recombine in the Qdisks' area. The thin p-$Al_xGa_{1-x}N$ layer on the active region provides a better opportunity for photons to escape from the top surface. In addition, well-aligned Qdisks were observed across the length of the NWs because of the highly uniform height of the AlGaN NWs. Detailed scanning transmission electron microscopy (STEM) studies revealed the high crystalline quality and nanocluster formation in Qdisks, which helps to promote high carrier localization[22] and quantum confinement.[20,23] An AlGaN Qdisk-in-NW LED that emitted at 303 nm at room temperature was demonstrated. A narrow linewidth emission spectrum was obtained at 48 A cm^{-2} bias (120 mA over an area of 0.5 × 0.5 mm^2) with a full width at half maximum (FWHM) of ~20 nm. The turn-on voltage was 9 V, and the rectification ratio was large for AlGaN Qdisk LEDs, which are comparable to the LEDs grown on Si substrates with similar emission wavelengths. The electroluminescent (EL) signal was collected with up to 200 mA DC injection using a UV objective. The Nextnano^3-based simulation showed an overlap of 42% in the strain-relieved 3D structure, which resulted in a high radiative recombination rate.

Experimental

The UV NW p–i–n LED structure was grown catalyst-free using the Veeco Gen 930 plasma-assisted molecular-beam epitaxy system (PAMBE). The native oxide was removed from Si (100) using a HF–H_2O solution. The Si wafer was first outgassed in the load lock at 200 °C using an infrared (IR) filament to remove any water component. Then, outgassing at 650 °C was performed in the buffer chamber to remove the organic-based contaminants. In the growth chamber, the wafer was ramped up to 900 °C for 30 min. Upon ramping down, the 1 × 1 surface reconstruction was observed at ~800 °C, which confirms the absence of any oxide layer. During this process, the wafer was kept facing away and was only brought in line with the sources immediately before the growth initiation. This maintained a uniform coverage of the pre-oriented silicon nitride (Si_3N_4) layer on the surface of Si substrates. The resulting orientation and density of the nucleated seeds will affect the height uniformity and the degree of coalescence as growth proceeds.

The key to achieving such nearly dislocation-free coalescence NWs is the precise control of the initial GaN nucleation process and growth conditions. The NW morphology and areal density can drastically change depending on the growth parameters such as: (a) NW areal density decreases with substrate temperature and increases with total metal flux;[24,25] (b) NW diameter increases with the density of active nitrogen species;[26] (c) NW height is inversely proportional to the substrate temperature;[24,26] (d) directionality of NWs depends on the nucleating or pre-orienting layers, such as AlN, and Si_3N_4; (e) a higher aspect ratio of NWs can be achieved with increasing flux ratio (V/III) and temperature[27] and (f) crystal polarity may be affected by the flux ratio, wetting layer and buffer layer.[28,29]

In this investigation, the Si-doped GaN layer (150 nm) was firstly nucleated on top of the silicon wafer at 690 °C to improve the crystal quality and achieve the required NW density. The aluminium flux was then increased to achieve compositional grading from GaN to $Al_{0.5}Ga_{0.5}N$ (over ~20 nm) and avoid any abrupt energy barrier for the electrons. Subsequently, a 75 nm Si-doped AlGaN layer was grown to provide a larger bandgap for the quantum confinement. The temperature was increased to 740 °C to grow the AlGaN layer. Then, an active region with 15 stacks of ~2.5 nm $Al_{0.3}Ga_{0.7}N$ Qdisks separated by ~7 nm $Al_{0.5}Ga_{0.5}N$ quantum barriers (QB) was grown on the n-AlGaN layer. For the active region, the Al flux was fixed at 2×10^{-8} Torr, whereas the Ga flux was alternated between 2×10^{-8} and 4.5×10^{-8} Torr for the QB and Qdisk, respectively. A 10 nm magnesium (Mg)-doped EBL layer was grown. Then, $Al_{0.6}Ga_{0.4}N$ was graded down to the GaN layer. As with the n-type AlGaN grading layer, grading (~20 nm) was performed to improve the hole injection and reduce absorption losses.[30–32] The device was completed with a 10 nm Mg-doped GaN layer as the p-type contact layer. The nitrogen flow was maintained at 1 sccm with a fixed RF power of 350 W to optimize the NW shape and density. A top-view scanning electron microscopy (SEM) image of the AlGaN NWs is shown in Fig. 1(a). The diameter and length of the NWs were measured to be ~70 and 400 nm, respectively.

SEM and TEM were used to investigate the quality and structure of the NWs. An FEI Titan 80–300 ST microscope was used for the TEM characterization. The microscope was operated at an accelerating voltage of 300 keV. The atomic-number-sensitive (*Z*-contrast) high-angle annular dark-field (HAADF) STEM images of the NWs were obtained. The strain field in the Qdisks was obtained using a geometrical phase analysis (GPA) analysis. The compositional variation of group-III

 This journal is © The Royal Society of Chemistry 2017

Published on 03 March 2017. Downloaded by King Abdullah Univ of Science and Technology on 31/08/2017 13:28:42.

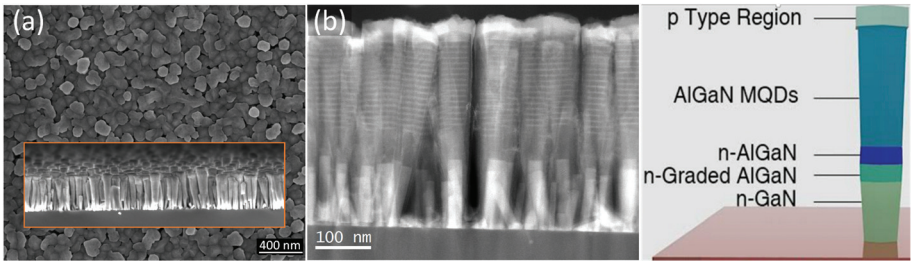

Fig. 1 (a) Top-view SEM image of the device structure, and tilted-angle SEM of the NWs in the inset; (b) STEM-HAADF image of the coalesced AlGaN NWs with the corresponding schematic showing the layer structure of the NW LED.

elements (Al $L_{2,3}$ and Ga $L_{2,3}$) and the Mg distribution in the NWs across different interfaces and layers were studied using elemental mapping by electron energy-loss spectroscopy (EELS) in the STEM mode. A weighted principal-components analysis (PCA) was applied to reduce the noise in the spectrum images using the MSA plugin in Digital Micrograph by HREM Research Inc.

Before the devices were fabricated, the room temperature photoluminescence (RTPL) was measured using a 266 nm excitation pulse laser (SNU-20F-100) in a reflective mode configuration. The PL signal was collected by a UV objective and beam splitter and subsequently focused into the Andor monochromator (SR-750). A 266 nm notch filter was used to filter off laser radiation. A cooled (−80 °C) iDUS silicon detector, which was connected to the monochromator, was used to measure the signal.

The UV NW LEDs were modeled using the commercial Nextnano^3 software.[33] The band diagram of the structure was obtained by self-consistently solving Poisson's, Schrödinger's, current continuity, and carrier transport equations under forward bias. For the valence band, the 6 × 6 *k·p* method was used to consider the non-parabolic nature of the energy bands. The effects of the wave function overlap, carrier dynamics in the AlGaN-based active region and polarization-induced band bending because of the interface fixed charges were also considered.

The UV NW LEDs were fabricated using the standard UV contact lithography process. First, the NWs were cleaned with a buffered oxide etch (BOE) solution to remove any oxide layer formation. Ni (15 nm)/Au (10 nm) layers were directly deposited on top of the coalesced p-GaN layer without a planarization process, which formed an ohmic contact with p-GaN, upon annealing at 600 °C in O_2 gas for 1 min. The thickness of the Ni/Au layer was used to spread the current well while being transparent to emitted UV light. Then, a thick Ni (10 nm)/Au (1 um) layer was deposited as the top p-contact pad for probing silicon was etched 200 nm from the back to expose a clean, unoxidized surface. For the back contact, Ti (10 nm)/Au (150 nm) were sputtered as the n-pad. Then, the device was annealed again in N_2 gas at 250 °C for 1 min to form an n-type ohmic contact. The electroluminescent (EL) signal was measured using the PL setup with a camera attached to the beam splitter mount. A Keithley source 2450C device was used to inject a continuous current into the device.

Results and discussion

Fig. 1(a) includes a high-magnification and cross-sectional SEM (CSSEM) image of AlGaN NWs. The coalescence of the top p-GaN layer is observed. This configuration improves the current spreading and injection and reduces carrier leakage without filling and planarizing materials, such as polyimide or parylene, which are commonly used in the fabrication process of NW-based devices.[34,35] The CSSEM image clearly shows that the NWs were largely vertically aligned along the *c*-axis and had a uniform height distribution over a large area. A high density of ~1×10^{10} cm^{-2} of NWs with a filling factor above 95% was estimated. Fig. 1(b) provides a schematic diagram of the detailed structure of the NW UV LED and an HAADF cross-sectional image of an array of AlGaN NWs. The brighter regions correspond to the Ga-heavy areas, which are the bottom n-type GaN, AlGaN/AlGaN Qdisk active regions, and the top p-GaN layer. The NWs were vertically aligned and closely spaced but disjointed along the active region, which demonstrates the good growth conditions. No threading dislocation or stacking faults were observed.

Fig. 2(a) shows the HAADF-STEM image of a single NW, which includes the n-type AlGaN layer, an active region, a p-type AlGaN electron-blocking layer (EBL), a top AlGaN grading layer and a p-GaN layer. Well-defined uniform 15 $Al_{0.3}Ga_{0.7}N$ Qdisks (2.5 nm) were sandwiched between $Al_{0.5}Ga_{0.5}N$ (7.1 nm) layers. The NWs exhibit an inverse tapered shape, where they are thinnest at the bottom (~30 nm) and have a diameter of 60 nm at the top. This shape was attributed to two main reasons: the variation in growth temperature as the growth proceeds and the slight lateral-growth preference because of the high Ga adatom mobility. A close examination of the NW sidewall shows the AlGaN encapsulation. This AlGaN shell has been reported to form because of the small diffusion length of aluminum, which promotes lateral growth.[5,6,36] When the NWs were grown, the growth temperature was stabilized before nucleation and the active region to ensure uniform Qdisks across the active region. No threading dislocation and stacking faults are observed. Fig. 2(b) shows a further study on the formation of nanoclusters in each Qdisk. The Ga-map (displayed on the temperature scale) and the concurrently acquired ADF signal from nanoscale EELS spectrum imaging (EELS-SI) (boxed in the blue dashed line in Fig. 2(b))

Published on 03 March 2017. Downloaded by King Abdullah Univ of Science and Technology on 31/08/2017 13:28:42.

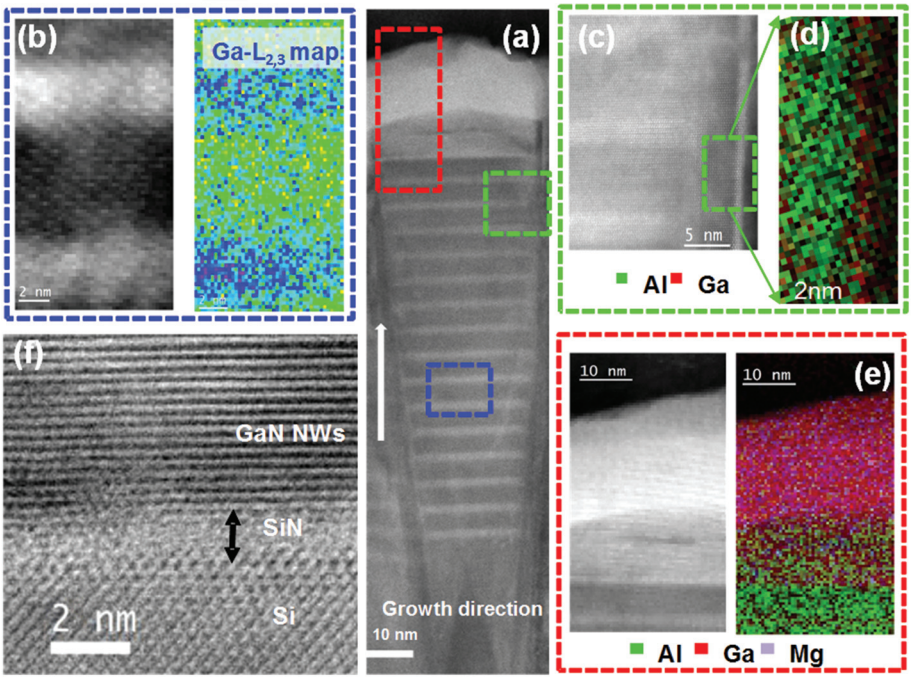

Fig. 2 (a) HAADF-STEM image of single NWs. (b) Concurrently acquired ADF signal and Ga-map from nanoscale EELS-SI (boxed in the blue dashed line in (a)), which show a direct correspondence between the local increases in the Ga signal and ADF signal within the signal atomic planes. (c) High-magnification atomic-resolution HAADF image of the selected region (boxed in the green dashed line) in (a). (d) Elemental mapping from the EELS spectrum in the green area marked in (c). (e) Elemental mapping from EELS-SI of the red area marked in (a) of group-III elements, which were extracted from Ga $L_{2,3}$, Al $L_{2,3}$, the acceptor Mg $L_{2,3}$ and the concurrently acquired ADF signal from nanoscale EELS-SI. (f) High-magnification atomic-resolution image of the interface between the GaN NW and the silicon (001) substrate.

show a direct correspondence between the local increases in the Ga signal and ADF signal in the signal atomic planes. This correspondence indicates the formation of nanoclusters in Qdisks, which might cause a strong quantum confinement effect related to the compositional fluctuations of the active region. Planar InGaN-based LEDs have been reported to achieve high efficiency because of the highly localized excitons, which are created by indium segregation.[37] Thin-film AlGaN-based UV light-emitting devices have achieved large optical gains with an extremely low optical pumping threshold *via* the introduction of high-density nanocluster-like features in the AlGaN wells.[38] Strong stimulated emission[22] and high-efficiency LEDs were produced by containing nanometer-scale compositional inhomogeneities in AlGaN thin films. Recently, the quantum-dot-like behavior of the compositional fluctuations[39] and three-dimensional quantum confinement in AlGaN double heterostructure NWs has been observed in achieving UV light emitters.[6] This work clearly demonstrates that high-crystal-quality AlGaN NWs with nanoclusters embedded in Qdisks can be widely applicable to achieve high-efficiency LEDs. Fig. 2(c) shows a high-magnification atomic-resolution HAADF image of the selected region (boxed in the green dashed line) in Fig. 2(a). This image presents a typical AlGaN core–shell structure (low Al content in the core of the NW and high Al content near the surface of the NW (dark region)). This Al-rich AlGaN shell was further surrounded by a few-atomic-plane-thick Ga-rich AlGaN outermost shell. The formation of the AlGaN shell was mainly ascribed to the Al adatom migration, which occurred more slowly than that of Ga adatoms and caused Al accumulation along the NW surface. This shell was further confirmed in Fig. 2(d), which shows the elemental mapping of the Ga $L_{2,3}$ and Al $L_{2,3}$ edges from EELS-SI of the green area in Fig. 2(c), which confirms the formation of an AlGaN core–shell structure. As reported by others, the formation of such Al-rich AlGaN in the near-surface region can improve the carrier confinement, reduce the surface states because of the self-passivated layer, and significantly suppress the nonradiative surface recombination, which results in a high internal quantum efficiency of 70–80% for the NW LEDs and lasers.[5] Fig. 2(e) shows an elemental mapping from the EELS-SI of the red area in Fig. 2(a). The elements extracted from Ga $L_{2,3}$, Al $L_{2,3}$, the acceptor Mg $L_{2,3}$ and the concurrently acquired ADF signal from nanoscale EELS-SI show the Ga and Al elemental distributions in different layers (red for Ga atoms, green for Al atoms, and purple for Mg atoms). The EELS mapping confirms the gradual decrease in Al content and the continuous increase in Ga content in the compositional graded p-AlGaN layer. The temperature of the Al source was linearly reduced to achieve a logarithmic decrease in aluminum flux; thus, an AlGaN grading layer was obtained. This graded p-AlGaN served as a transition layer to avoid creating a high abrupt potential for the holes to inject into the Qdisks while maintaining a small p-GaN thickness to mitigate reabsorption losses. Fig. 2(f)

 This journal is © The Royal Society of Chemistry 2017

Published on 03 March 2017. Downloaded by King Abdullah Univ of Science and Technology on 31/08/2017 13:28:42.

shows a high-magnification atomic-resolution image of the interface between the GaN NW and the silicon (100) substrate. There is an extremely thin (1–2 nm) Si_3N_4 monolayer at the GaN NW and silicon interface during the initial nucleation stage. The Si_3N_4 formation is thermodynamically favored, which is commonly observed when similar GaN NWs are directly grown on Si. The thickness of Si_3N_4 was minimized by bringing the substrate into a position facing the sources immediately before the growth.

To understand the distribution of strain for Qdisks in AlGaN NWs, a GPA was applied to the HR-STEM image of Fig. 3(a) in the region inside the red lines in Fig. 2(a). The strain fields are the derivatives of the displacement fields along the x- and y-axes and can be defined as follows:

$$e_{xx} = \frac{\partial u_x(r)}{\partial x} = -\frac{1}{2\pi|g1|}\frac{\partial P_{g1}(r)}{\partial x} \quad (1)$$

$$e_{yy} = \frac{\partial u_y(r)}{\partial y} = -\frac{1}{2\pi|g2|}\frac{\partial P_{g2}(r)}{\partial y} \quad (2)$$

where e_{xx}, e_{yy}, $u_x(r)$, $u_y(r)$, $g1$, $g2$, $P_{g1}(r)$, and $P_{g2}(r)$ are the in-plane biaxial strains, out-of-plane strain (along the growth direction), displacement field along x, displacement field along y, reciprocal vector along x, reciprocal vector along y, and the corresponding phase images, respectively.[40,41]

The GPA analysis based on the above formulation was applied to the HAADF-HRSTEM image to determine the strain fields in the AlGaN NWs. The HAADF-HRSTEM image of three Qdisks is shown in Fig. 3(a), and the corresponding GPA result is shown in Fig. 3(b). Because the strain is considerably relieved in the thick n-AlGaN layer, the strain was referenced to the AlGaN barrier, which was assumed to be strain-free. Strain-free AlN NWs have been shown to grow on Si.[42] The results in Fig. 3(b) show that a slight build-up of strain is observed in the Qdisks along the growth direction, which is as expected. In addition, the strain in the growth direction was quantified by generating a line profile across the dotted areas in the strain map. The increase in strain in the upper Qdisks may be because of the increase of the total strained Qdisk volume in the growth direction. In addition, the increase in the width of the NWs may increase the strain in the Qdisk as the growth proceeds. Nevertheless, the strain in our AlGaN NWs is considerably smaller than the planar structures with a similar Al composition, which paves a new way for achieving highly efficient UV emitters.

The strain in the free-standing NW was calculated as shown in Fig. 3(d). The Qdisks have biaxial tensile strain in the presence of the bottom n-GaN layer. The out-of-plane strain of 0.00019 corresponds well with the measured ~0.0002 strain, as shown in Fig. 3(c). Because the model adopted for calculations minimizes the strain energy at the interface of n-GaN/AlGaN, n-GaN is compressively strained, whereas n-AlGaN is tensile strained.

Next, we investigated the optical properties of AlGaN Qdisks in NWs. A 3-dimensional (3D) schematic diagram of the NWs with the respective layers is shown in Fig. 4(a). Fig. 4(b) shows

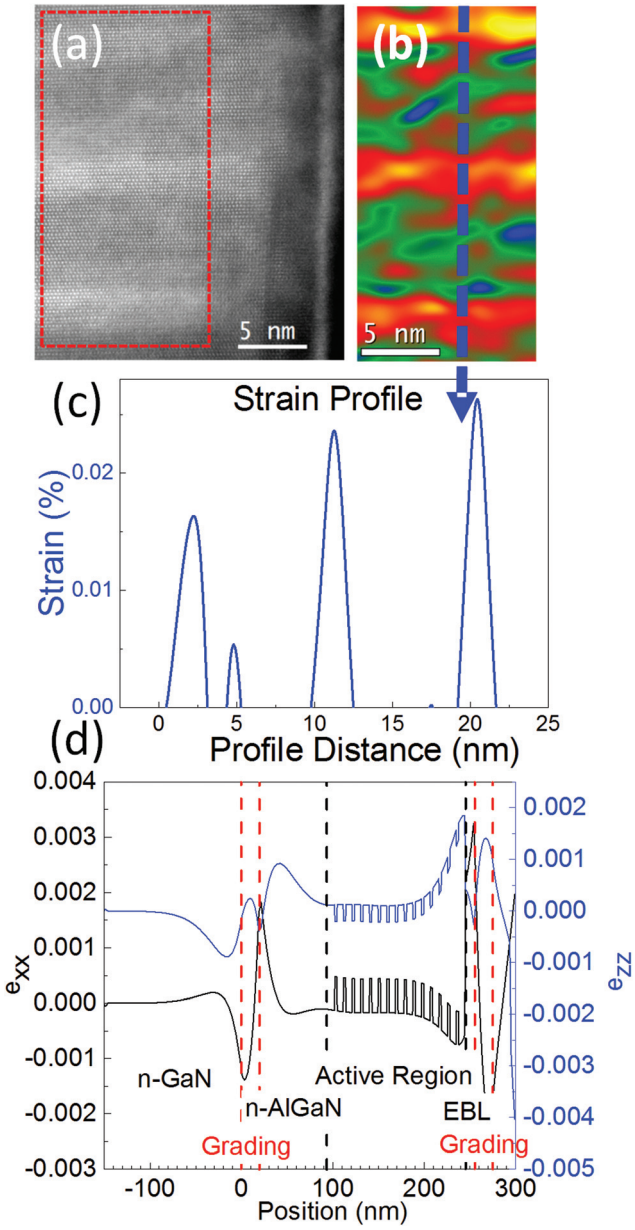

Fig. 3 (a) HAADF-HRSTEM images of the three top Qdisks, which are identical to the area enclosed in the green dashed box in Fig. 2(a). (b) Strain map obtained using a geometrical phase analysis for the selected area. (c) Strain profile of the three Qdisks. (d) Simulated biaxial and uniaxial strain of a free-standing NW.

the room-temperature PL of the AlGaN NWs. A strong PL signal is an indication of the quantum confinement in Qdisk structures with good AlGaN crystalline quality. The spectrum consists of three Gaussian peaks, which could originate from different layers in the NW. The three peaks that emit at ~303, ~314, and ~356 nm at room temperature correspond to the emissions from the active region, graded layer, and GaN contact layer, respectively. The emission from the active region has an FWHM of 14.8 nm, which is related to highly localized carriers in the Qdisks. In reported UV devices based on DHS, it

Published on 03 March 2017. Downloaded by King Abdullah Univ of Science and Technology on 31/08/2017 13:28:42.

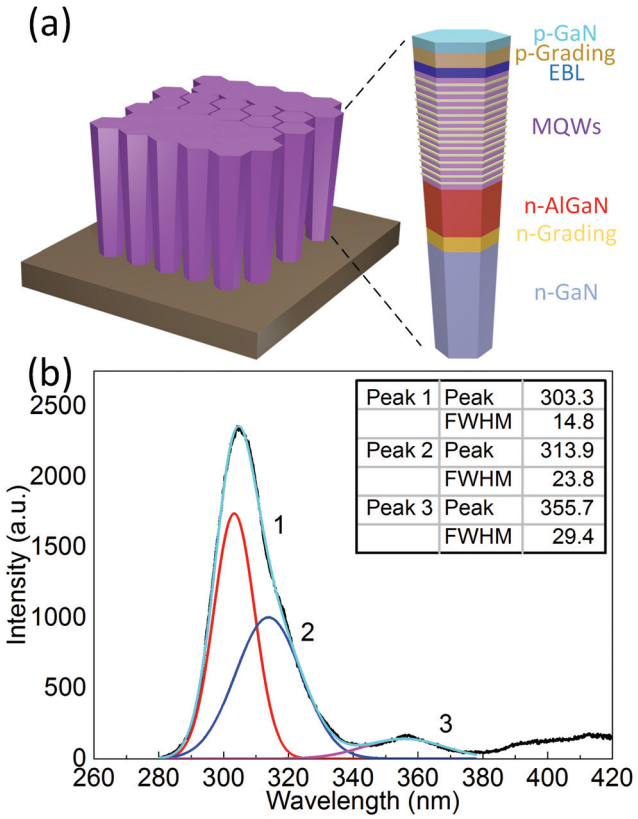

Fig. 4 (a) 3D depiction of the UV-emitting NWs with individual layers labeled. (b) RTPL spectrum with peak intensities at ~303, ~314 and ~356 nm, which were emitted from the active region, graded AlGaN layer, and top and bottom GaN layers. Red, blue and green are the Gaussian fit spectra for the three peaks.

was shown to have a considerably broader linewidth than that of this investigation, thus highlighting the advantage of using quantum-confined structures.[36] The AlGaN material is less prone to temperature variations than InGaN, which has been shown to have a FWHM of more than 50 nm.[43] PL peaks from the graded AlGaN layer and GaN layer have considerably broader FWHMs of 23.8 and 29.4 nm, respectively. This is likely due to the dopant-dependent linewidth broadening and therefore the band-tailing effect, as well as the bandgap variation in the presence of inhomogeneous strain; both effects becoming more prominent with the increase in layer thickness. As discussed below, the peak at ~303 nm correlates well with the EL emission at high current injection. A broad but relatively weak peak at approximately 400 nm indicates the recombination through the trap states introduced by Mg impurities in GaN.[44]

The NWs nucleate *via* strain relaxation through their free surface.[45,46] Strain was adjusted in the 1D model to depict the more realistic free standing scenario as shown in Fig. 3(d). In the simulation, the growth direction was assumed to be N-polar, which is an important parameter in determining the direction of polarization fields.[47] The band offsets $\Delta E_c/\Delta E_v$ were assumed to be 70/30.[48] Fig. 5(a) shows the calculated band diagram of the AlGaN Qdisk-based UV NW LED under a forward bias of 4 V. Fig. 5(b) shows a considerably large wave function overlap of 42% for the electrons and holes because of the suppressed piezo-polarization fields, as shown in Fig. 5(c). The calculated recombination rates in the active region show that the SRH and direct radiative recombination are dominant (Fig. 5(d)). With a further increase in voltage bias, the direct radiative recombination rate is expected to surpass the SRH non-radiative recombination. On the other hand, because of the large number of wells, and reduced average carrier density, the Auger recombination is significantly suppressed. The energy separation of 4.19 eV (296 nm) between the confined carrier states correlates well with the PL and EL peak positions (303.3 nm). A decrease in barrier height is observed by 0.22 eV and 0.3 eV at n-$Al_{0.5}Ga_{0.5}N$/GaN and p-$Al_{0.6}Ga_{0.4}N$/GaN interfaces by incorporating a graded layer compared to the conventional abrupt interface, which can significantly enhance the carrier injection efficiency of our device.

Fig. 6(a) presents the current–voltage characteristics of the AlGaN NW LED on a linear scale. The good diode behavior with a turn-on voltage of 9 V and a large rectification ratio (ratio of the forward bias to the reverse bias current) of ~10^6 at ±15 V are observed. In the presence of the adopted coalesced top p-GaN growth scheme, our device shows improved reverse bias behavior compared to the more commonly used tilted-angle deposition technique for realizing devices emitting around 300 nm or below.[5,7] The larger turn-on voltage of 9 V compared to the bandgap of the active region might be because of the Si_3N_4 layer at the GaN/Si interface, smaller p-contact area and reduced doping efficiency in large-bandgap AlGaN layers in these NWs. In studies on NWs, turn-on voltages of ~5 V to ~12 V have been reported with a significant improvement obtained when using tunnel junctions.[7,19,21,49] In comparison, a planar structure having GaN/AlN embedded quantum-dots, emitting at 308 nm, with an estimated IQE of 62% was demonstrated albeit with a considerably larger turn-on voltage of 14 V.[50] This further highlights the efficient doping in NW-based devices. The optical power at different injection currents can be derived from the *L–I* measurement, as shown in Fig. 6(a). It may be necessary to have a stable light output power at high injection levels based on the practical application. The conventional nitride-based planar devices suffer from the "efficiency-droop" phenomenon, which is a degradation of the optical power with an increase in injection current.[44] As shown in Fig. 6(b), which depicts the calculated EQE plotted against the current, a droop is observed up to an injection current of 80 mA cm^{-2}. The device performance can be improved because our device may have the following issues: (1) reduced photon collection efficiency because the device under testing was not placed inside the integrating sphere; (2) low light extraction efficiency in the presence of a top metal pad shadow, which covered 40% of the device area, semi-transparent Ni (15 nm)/Au (10 nm) spreading layer and the absorbing top p-GaN layer; and (3) poor heat dissipation and current injection in the presence of Si_3N_4 formation. All of these issues can be resolved with further structure design, growth

 This journal is © The Royal Society of Chemistry 2017

Published on 03 March 2017. Downloaded by King Abdullah Univ of Science and Technology on 31/08/2017 13:28:42.

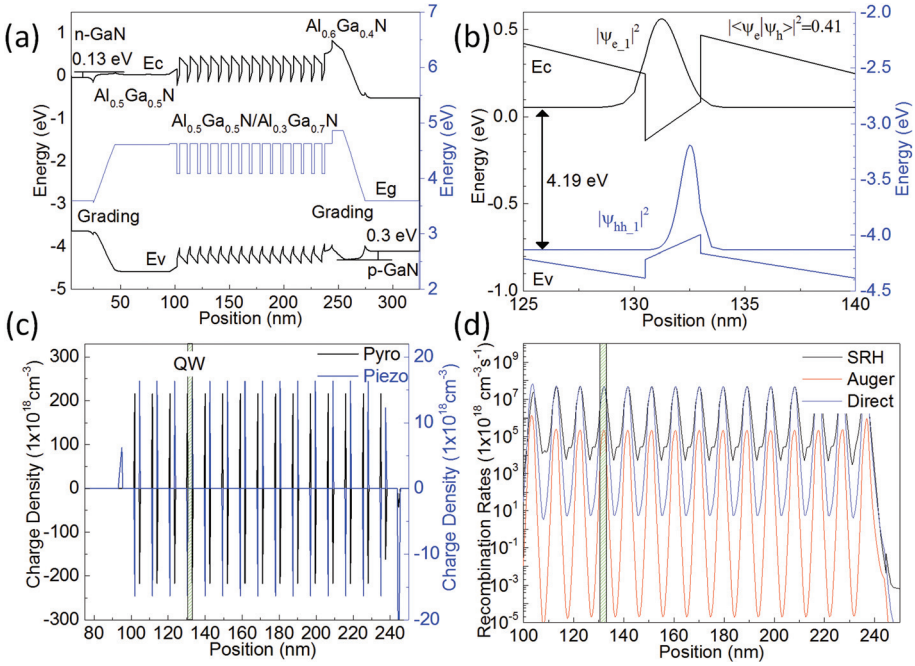

Fig. 5 (a) Band diagram under a forward bias of 4 V. (b) Wave function profiles that correspond to the electrons and holes in the active region. (c) Polarization-induced fixed charges. (d) Recombination rates including Shockley–Read–Hall (SRH), Auger and direct recombination in the active region. The fourth QW from the n-side is marked with a green box.

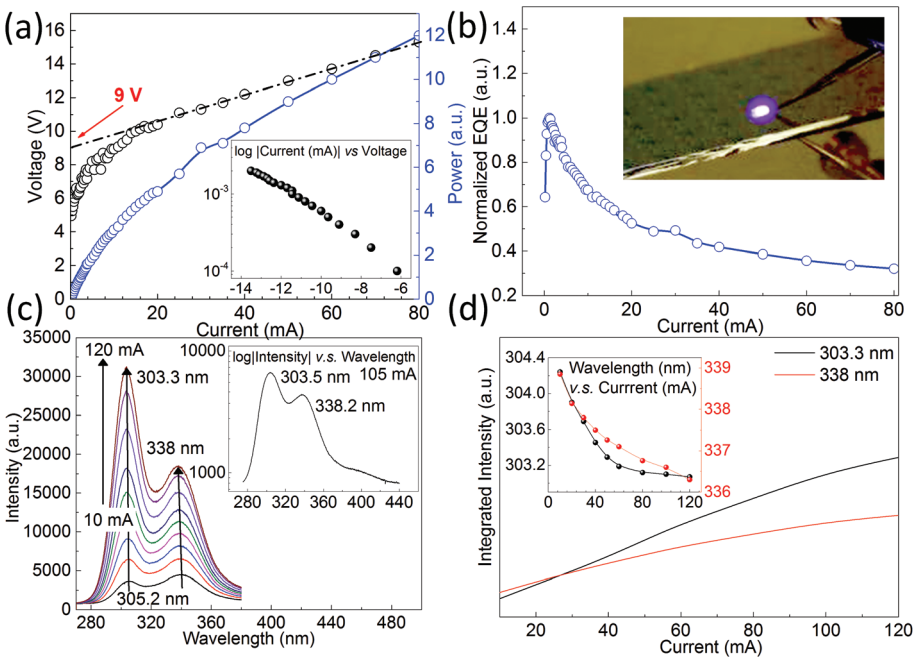

Fig. 6 (a) *L–I–V* characteristics of the NW UV LED, with the reverse bias characteristics shown in the inset. (b) The calculated EQE of the device. (c) The EL spectrum of the NW device with a changing current bias of 0–120 mA, and the measurement using an extended wavelength range showing the contribution from GaN (see the inset). (d) Variation of the integrated intensities and peak shifts (see the inset) of the two EL peaks.

optimization and device fabrication. A photograph of the lighting device is shown in the inset of Fig. 6(b).

The room temperature electroluminescence (EL) spectra of the AlGaN NW LEDs were collected at different injection currents of 1–120 mA, as shown in Fig. 6(c). The primary peak from the active region is ~303.3 nm with a slight blueshift (~1.4 nm) in the range of injected currents, as shown in the inset of Fig. 6(d). The logarithmic plot of the EL intensity,

Published on 03 March 2017. Downloaded by King Abdullah Univ of Science and Technology on 31/08/2017 13:28:42.

shown in the inset of Fig. 6(c), shows insignificant emission at approximately 400 nm, which indicates negligible current leakage into the p-GaN layer. A second peak at 338 nm is observed with an FWHM of ~39.2 nm. The large width of this peak indicates the electron–hole recombination process from the graded AlGaN layer.[18,19,51] A similar but relatively weaker peak is also observed in the RTPL spectrum. The integrated intensities of the two EL peaks under different injection currents further verify the origin of the two peaks (see the inset of Fig. 6(d)). At low injection current, because the mobility of the holes was lower than the mobility of the electrons, more electron–hole pairs were recombined in the graded AlGaN layer and fewer holes reached the Qdisks, which created a stronger 338 nm than the 303 nm peak from the active region. However, with an increase in bias current, increasingly more holes could reach the Qdisks and effectively recombine in these highly localized states. After the current was increased to 40 mA, the radiative recombination across the active region began to dominate, as indicated in the EL spectra. With a further increase in bias current, the peak intensity of 304 nm increased nearly linearly, whereas the peak at 338 nm began to saturate. Fig. 6(d) shows a similar trend of the integrated intensity of the two peaks. The optical performance can be further improved *via* device optimizations, such as tuning the thickness and Al concentration of the graded AlGaN layer or using large-bandgap insertion layers in the active region to increase the strength of the radiative recombination.[52]

Conclusions

In summary, UV-B LEDs based on self-planarized AlGaN NWs with embedded Qdisks were demonstrated. The vertically aligned NWs with a large density of $\sim 1 \times 10^{10}$ cm^{-2} and coalesced top p-GaN were grown using PAMBE on Si substrates with a large filling factor (>95%). Strong PL and EL emissions from the active region were obtained because of the good crystal quality of the material, reduced polarization fields, and tightly quantum-confined carriers in the Qdisks-in-NWs. The EL peak emission of the Qdisk-based UV LEDs has a small linewidth of 20 nm, which is significantly smaller than that of the conventional DHS-based UV NW LEDs.

Acknowledgements

We acknowledge the financial support from the King Abdulaziz City for Science and Technology (KACST), Grant No. KACST TIC R2-FP-008. This work was partially supported by the King Abdullah University of Science and Technology (KAUST) baseline funding, BAS/1/1614-01-01.

Notes and references

1 A. Khan, K. Balakrishnan and T. Katona, *Nat. Photonics*, 2008, **2**, 77–84.
2 S. H. Park and S. L. Chuang, *Phys. Rev. B: Condens. Matter*, 1999, **59**, 4725–4737.
3 H. P. Zhao, G. Y. Liu, J. Zhang, J. D. Poplawsky, V. Dierolf and N. Tansu, *Opt. Express*, 2011, **19**, A991–A1007.
4 M. Shatalov, W. H. Sun, A. Lunev, X. H. Hu, A. Dobrinsky, Y. Bilenko, J. W. Yang, M. Shur, R. Gaska, C. Moe, G. Garrett and M. Wraback, *Appl. Phys. Express*, 2012, **5**, 082101.
5 S. Zhao, A. T. Connie, M. H. T. Dastjerdi, X. H. Kong, Q. Wang, M. Djavid, S. Sadaf, X. D. Liu, I. Shih, H. Guo and Z. Mi, *Sci. Rep.*, 2015, **5**, 8332.
6 K. H. Li, X. Liu, Q. Wang, S. Zhao and Z. Mi, *Nat. Nanotechnol.*, 2015, **10**, 140–144.
7 S. Zhao, S. Y. Woo, M. Bugnet, X. Liu, J. Kang, G. K. Botton and Z. Mi, *Nano Lett.*, 2015, **15**, 7801–7807.
8 S. Zhao, X. Liu, S. Y. Woo, J. Kang, G. A. Botton and Z. Mi, *Appl. Phys. Lett.*, 2015, **107**, 043101.
9 A. T. Connie, S. R. Zhao, S. M. Sadaf, I. Shih, Z. Mi, X. Z. Du, J. Y. Lin and H. X. Jiang, *Appl. Phys. Lett.*, 2015, **106**, 213105.
10 M. Djavid and Z. Mi, *Appl. Phys. Lett.*, 2016, **108**, 051102.
11 Q. Wang, H. P. T. Nguyen, K. Cui and Z. Mi, *Appl. Phys. Lett.*, 2012, **101**, 043115.
12 D. Gonzalez, R. Fath, T. Ben and R. Songmuang, 2011, arXiv preprint arXiv:1107.0846.
13 H. P. T. Nguyen, M. Djavid, S. Y. Woo, X. H. Liu, A. T. Connie, S. M. Sadaf, Q. Wang, G. A. Botton, I. Shih and Z. Mi, *Sci. Rep.*, 2015, **5**, 7744.
14 C. Zhao, T. K. Ng, N. N. Wei, A. Prabaswara, M. S. Alias, B. Janjua, C. Shen and B. S. Ooi, *Nano Lett.*, 2016, **16**, 1056–1063.
15 B. Janjua, H. Sun, C. Zhao, D. H. Anjum, D. Priante, A. A. Alhamoud, F. Wu, X. Li, A. M. Albadri, A. Y. Alyamani, A. Y. Alyamani, M. M. El-Desouki, T. K. Ng and B. S. Ooi, *Opt. Express*, 2017, **25**, 1381–1390.
16 B. H. Le, S. Zhao, X. Liu, S. Y. Woo, G. A. Botton and Z. Mi, *Adv. Mater.*, 2016, **28**, 8446–8454.
17 H. Sekiguchi, K. Kato, J. Tanaka, A. Kikuchi and K. Kishino, *Phys. Status Solidi A*, 2008, **205**, 1067–1069.
18 T. F. Kent, S. D. Carnevale, A. T. M. Sarwar, P. J. Phillips, R. F. Klie and R. C. Myers, *Nanotechnology*, 2014, **25**, 455201.
19 S. D. Carnevale, T. F. Kent, P. J. Phillips, M. J. Mills, S. Rajan and R. C. Myers, *Nano Lett.*, 2012, **12**, 915–920.
20 B. J. May, A. T. M. G. Sarwar and R. C. Myers, *Appl. Phys. Lett.*, 2016, **108**, 141103.
21 A. T. M. G. Sarwar, B. J. May, J. I. Deitz, T. J. Grassman, D. W. McComb and R. C. Myers, *Appl. Phys. Lett.*, 2015, **107**, 101103.
22 J. Mickevicius, J. Jurkevicius, K. Kazlauskas, A. Zukauskas, G. Tamulaitis, M. S. Shur, M. Shatalov, J. Yang and R. Gaska, *Appl. Phys. Lett.*, 2012, **101**, 041912.
23 A. T. M. G. Sarwar, B. J. May, M. F. Chisholm, G. J. Duscher and R. C. Myers, *Nanoscale*, 2016, **8**, 8024–8032.
24 M. Yoshizawa, A. Kikuchi, M. Mori, N. Fujita and K. Kishino, *Jpn. J. Appl. Phys., Part 2*, 1997, **36**, L459–L462.

 This journal is © The Royal Society of Chemistry 2017

Published on 03 March 2017. Downloaded by King Abdullah Univ of Science and Technology on 31/08/2017 13:28:42.

25 S. D. Carnevale, J. Yang, P. J. Phillips, M. J. Mills and R. C. Myers, *Nano Lett.*, 2011, **11**, 866–871.
26 R. Calarco, R. J. Meijers, R. K. Debnath, T. Stoica, E. Sutter and H. Luth, *Nano Lett.*, 2007, **7**, 2248–2251.
27 S. Fernandez-Garrido, X. Kong, T. Gotschke, R. Calarco, L. Geelhaar, A. Trampert and O. Brandt, *Nano Lett.*, 2012, **12**, 6119–6125.
28 K. Hestroffer, C. Leclere, C. Bougerol, H. Renevier and B. Daudin, *Phys. Rev. B: Condens. Matter*, 2011, **84**, 245302.
29 S. D. Carnevale, T. F. Kent, P. J. Phillips, A. T. M. G. Sarwar, C. Selcu, R. F. Klie and R. C. Myers, *Nano Lett.*, 2013, **13**, 3029–3035.
30 H. Sun and T. D. Moustakas, *Appl. Phys. Express*, 2013, **7**, 012104.
31 H. Sun, J. Woodward, J. Yin, A. Moldawer, E. F. Pecora, A. Y. Nikiforov, L. Dal Negro, R. Paiella, K. Ludwig Jr. and D. J. Smith, *J. Vac. Sci. Technol., B: Nanotechnol. Microelectron.: Mater., Process., Meas., Phenom.*, 2013, **31**, 03C117.
32 B. Janjua, T. K. Ng, A. Y. Alyamani, M. M. El-Desouki and B. S. Ooi, *IEEE Photonics J.*, 2014, **6**, 1–12.
33 S. Birner, T. Zibold, T. Andlauer, T. Kubis, M. Sabathil, A. Trellakis and P. Vogl, *IEEE Trans. Electron Devices*, 2007, **54**, 2137–2142.
34 Y. S. Jeong, B. Ratier, A. Moliton and L. Guyard, *Synth. Met.*, 2002, **127**, 189–193.
35 A. Georgiev, D. Dimov, E. Spassova, J. Assa, G. Danev and P. Dineff, *Chemical and Physical Properties of Polyimides: Biomedical and Engineering Applications*, 2012.
36 Q. Wang, A. T. Connie, H. P. T. Nguyen, M. G. Kibria, S. Zhao, S. Sharif, I. Shih and Z. Mi, *Nanotechnology*, 2013, **24**, 345201.
37 A. Kikuchi, M. Kawai, M. Tada and K. Kishino, *Jpn. J. Appl. Phys., Part 2*, 2004, **43**, L1524–L1526.
38 E. F. Pecora, W. Zhang, J. Yin, R. Paiella, L. Dal Negro and T. D. Moustakas, *Appl. Phys. Express*, 2012, **5**, 032103.
39 M. Belloeil, B. Gayral and B. Daudin, *Nano Lett.*, 2016, **16**, 960–966.
40 Y. Y. Zhu, C. Ophus, J. Ciston and H. Y. Wang, *Acta Mater.*, 2013, **61**, 5646–5663.
41 P. Mishra, B. Janjua, T. K. Ng, D. H. Anjum, R. T. Elafandy, A. Prabaswara, C. Shen, A. Salhi, A. Y. Alyamani, M. M. El-Desouki and B. S. Ooi, *Opt. Mater. Express*, 2016, **6**, 2052–2062.
42 Q. Wang, S. Zhao, A. T. Connie, I. Shih, Z. Mi, T. Gonzalez, M. P. Andrews, X. Z. Du, J. Y. Lin and H. X. Jiang, *Appl. Phys. Lett.*, 2014, **104**, 223107.
43 B. Janjua, T. K. Ng, C. Zhao, H. M. Oubei, C. Shen, A. Prabaswara, M. S. Alias, A. A. Alhamoud, A. A. Alatawi, A. M. Albadri, A. Y. Alyamani, M. M. El-Desouki and B. S. Ooi, *Opt. Express*, 2016, **24**, 19228–19236.
44 D. S. Shin, D. P. Han, J. Y. Oh and J. I. Shim, *Appl. Phys. Lett.*, 2012, **100**, 153506.
45 O. Landre, D. Camacho, C. Bougerol, Y. M. Niquet, V. Favre-Nicolin, G. Renaud, H. Renevier and B. Daudin, *Phys. Rev. B: Condens. Matter*, 2010, **81**, 153306.
46 A. A. Darhuber, T. Grill, J. Stangl, G. Bauer, D. J. Lockwood, J. P. Noel, P. D. Wang and C. M. S. Torres, *Phys. Rev. B: Condens. Matter*, 1998, **58**, 4825–4831.
47 P. J. Phillips, S. D. Carnevale, R. Kumar, R. C. Myers and R. F. Klie, *ACS Nano*, 2013, **7**, 5045–5051.
48 J. Piprek, *Nitride semiconductor devices: principles and simulation*, John Wiley & Sons, 2007.
49 Z. Mi, S. Zhao, A. Connie and M. H. T. Dastjerdi, SPIE OPTO, International Society for Optics and Photonics, 2015, pp. 937306–937306.
50 W. Yang, J. Li, Y. Zhang, P.-K. Huang, T.-C. Lu, H.-C. Kuo, S. Li, X. Yang, H. Chen and D. Liu, *Sci. Rep.*, 2014, **4**, 5166.
51 J. P. Zhang, A. Chitnis, V. Adivarahan, S. Wu, V. Mandavilli, R. Pachipulusu, M. Shatalov, G. Simin, J. W. Yang and M. A. Khan, *Appl. Phys. Lett.*, 2002, **81**, 4910–4912.
52 B. Janjua, T. K. Ng, A. Y. Alyamani, M. M. El-Desouki and B. S. Ooi, *IEEE Photonics J.*, 2014, **6**, 1–9.